T.2: Pulsed laser deposition: a versatile process to grow advance materials

Pankaj Misra* and Bijendra Singh
Laser Materials Processing Division
**E-mail: pmisra@rrcat.gov.in*

Abstract

One of the most significant aspects of nano-technology is to fabricate material structures of nanometer size with comprehensive control on shape, dimensionality, size and size dispersion etc. Among a host of vacuum based growth methodologies available today, the pulsed laser deposition (PLD), which is an advanced application of lasers in materials science, has emerged as one of the most amenable and versatile technique to grow nanostructures of different materials under variety of conditions and with varying degrees of control. We, at LMPD, RRCAT, have created a versatile PLD facility based on KrF excimer laser for growing nanostructures of various materials with deterministic characteristics for cutting edge technological applications. Some of these include multilayer stacked ZnO quantum dots for UV-blue light emitting applications, ultra-thin films of ternary Lanthanides for miniaturized logic devices, nanostructured metal oxide films for resistive switching memories etc. Details of growth of these nanostructured materials using PLD and their characterizations for particular application are discussed in this article.

1. Introduction

One of the most significant aspects of modern material science and nanotechnology is to fabricate complex material structures of nanometer size with comprehensive control on dimensionality, size, shape, and size/shape dispersion etc [1, 2]. The commonly used method to grow different class of nanostructured materials includes wet chemical methodology. However, the wet chemical methodology suffers from serious limitations particularly when it comes to growing nanostructured materials of complex compositions for device applications. Thus a vacuum based growth methodology is needed for fabricating device grade nanostructures of complex compositions. Among a host of vacuum based growth methodologies available to grow nanometer size structures of different materials under variety of conditions and with varying degrees of controls, the Pulsed Laser Deposition (PLD) is a technique which is one of the most amenable to the research environment [2, 3] and highly suitable for growth of complex oxide materials. PLD is an advanced application of lasers in materials science.

At the initial stages of 'nanofabrication' of structures for particular device application, materials scientists were apprehensive about the use of PLD for growing nanometer size structures primarily because of its inherent limitations i.e. particulate production, small area deposition and high average kinetic energy of the plume particles resulting from laser ablation of the target material [2, 3]. However, despite its innate limitations there is an optimized regime of growth parameters in which this technique can indeed be applied for fabrication of high quality nanostructures. In this article, we will discuss in brief the fundamental aspects of PLD, the available level of technology, its merits and demerits and a perspective of the existing trends of this versatile fabrication methodology.

2. Fundamentals of pulsed laser deposition

Pulsed laser deposition is one of the popular growth methodologies to deposit variety of technologically important nano-structured materials under optimized conditions. Schematic of PLD setup is shown in Fig. T.2.1. The technique uses high power and short laser pulses to ablate materials from their high density targets. This ablation event produces a transient, highly luminous plasma plume that expands rapidly away from the target surface. The ablated material is condensed on a solid substrate resulting in the formation of quantum structures or the bulk like thin films depending upon the time and other conditions of deposition. The growth process may be supplemented by a passive or a reactive ambient and under optimal conditions of deposition, the ratio of the chemical composition of the target and the grown film can be the same. Due to its extreme simplicity, congruent evaporation and ease in handling reactive oxygen, PLD has emerged as a popular choice for the growth of complex oxide materials [2-4].

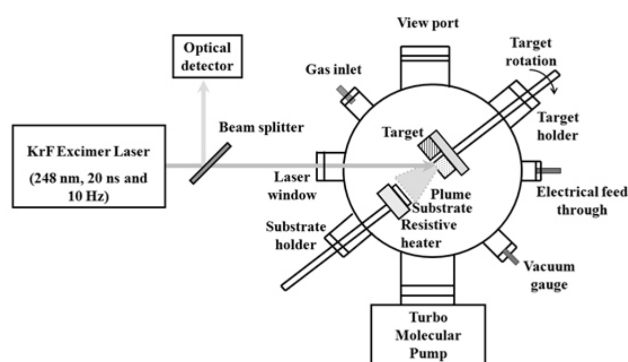

Fig. T.2.1: Schematic of PLD setup including vacuum chamber and KrF excimer laser

As mentioned earlier, in PLD process the energy source, which creates the plasma plume of the target material, the laser, is independent of the deposition setup. This in turn produces enormous facility in the growth of complex multilayer thin films which is possible within a single system simply by exposing individual targets one by one in sequential fashion. The useful range of laser wavelength for high quality materials' growth is ~200 - 400 nm. This is due to the fact that for most of the oxide materials, the absorption coefficient tends to increase with decreasing laser wavelength and material exhibits strong surface absorption of light in the UV spectral range thereby reducing particulate generation. The stronger absorption in the UV spectral range results in the reduced threshold fluence for the ablation process. Within the desired UV spectral range there are few laser systems which can deliver required high energy density in large areas. The most popular choice for the lasers in PLD is Excimer lasers [2-4]. The Excimer laser is a gas laser system and emits radiation directly into UV spectral range without using any nonlinear crystals [3, 5]. Pulsed KrF and XeCl lasers (pulse width few tens of ns) operating at 248 and 308 nm respectively are the most preferred for PLD applications due to their high gain [5]. Another possibility is the frequency multiplied solid state lasers such as $3^{rd}/4^{th}$ harmonic of Q-switched Nd: YAG laser [2, 3] at 355 and 244 nm respectively.

Fig. T.2.2: Image of PLD setup at LMPD, RRCAT consisting of KrF excimer laser and PLD chambers.

At LPMD, RRCAT, we have KrF Excimer laser based PLD systems for growth of a broad range of nanostructured materials and various characterization techniques to investigate their optical and electrical properties and suitability for particular device application. The image of PLD system at our laboratory is shown in Fig. T.2.2. It consists of a KrF excimer laser capable of providing 20 ns laser pulses at variable repetition rate up to 50 Hz with energy per pulse up to about 800 mJ at 248 nm. During PLD process the laser beam is zapped on the target and the generated plume is allowed to condense on a substrate, which is mounted on an electrical heater to control growth temperature. Since the laser ablation results in congruent evaporation, multi-component materials can be deposited with nearly the same stoichiometry as in the target. Further the rate of evaporation per pulse can be kept so low by controlling laser energy that one can deposit a layer with control on thickness as fine as 0.1Å per pulse. The PLD process is carried out in a growth chamber, which is first evacuated to a base pressure of ~ 10^{-8} Torr using a turbomolecular pump and can later be filled with flowing gaseous ambient required for different deposition conditions. For reactive deposition of oxides, high purity oxygen ambient is used, while inert gasses like Ar_2 and N_2 are used for plume cooling during deposition. In PLD a high density target of high purity material is needed for ablation. We have in-house facility for making high purity and high density targets by conventional ceramic route. After deposition of the nanostructured materials and routine structural, morphological and compositional characterizations, their optical and electrical properties are studied by absorption and temperature dependent photoluminescence spectroscopy, current-voltage, capacitance-voltage and temperature dependent Hall measurements etc. For other characterizations we collaborate with groups within and outside RRCAT.

3. Research areas and findings

We now discuss in brief few specific examples of pulsed laser deposition of technologically important metal oxide nanostructures and their characterizations which may have direct implication in modern device applications. These include multilayered stacks of Alumina capped ZnO quantum dots for photonic applications, $ZnO/Mg_xZn_{1-x}O$ hetero-structures and associated 2D electron gas for transparent electronic applications, ultra-thin and amorphous films of high k dielectric rare earth ternary oxide $LaGdO_3$ for CMOS gate dielectric application in nano-electronics and ultrathin films of binary metal oxides NiO and ternary rare earth oxide $SmGdO_3$for resistive switching non-volatile memory applications. The findings of our research in these fields have been published in a number of papers in peer reviewed journals and in international conference proceedings. A glimpse of our research findings in aforementioned area are presented below:

3.1 Multilayered stacks of ZnO quantum dots

As is well known, the current spurt of research in ZnO

quantum dots (QDs) is driven by an almost visible possibility of developing ZnO based low cost and energy efficient UV-blue and white light emitting devices and transparent logics [6, 7]. Due to the remarkable excitonic properties of bulk ZnO, which includes large exciton binding energy of ~60 meV and strong exciton-photon and exciton-phonon couplings, significant excitonic effects are expected in ZnO QDs on quantum confinement [8-10]. It is therefore imperative to realize ZnO QDs with efficient room temperature photoluminescence (PL) arising due to quantum size effects. Apart from these, research on QDs of ZnO is also interesting for the development of nano-regime sensors, catalytic and other chemical systems and photonic devices etc.

We have used sequential PLD to grow multilayered stacks of ZnO quantum dots of varying sizes in the range of ~ 3 to 1.6 nm capped with alumina matrix on sapphire substrates and investigated their room temperature photoluminescence properties. Prior to the deposition of ZnO QDs ~ 10 nm base layer of alumina was grown on the substrates over which were grown the randomly distributed QDs of ZnO of particular size distribution by controlling the ablation time of ZnO target. This layer of the ZnO QDs was then capped with alumina. A 10-layer structure of ZnO QDs and alumina capping layer was grown by the alternate ablation of the respective targets using KrF Excimer laser at a fluence of ~ 2 J/cm^2.

The detailed structural characterizations of ZnO QDs to study crystallinity, shape, and size distribution using transmission electron microscopy (TEM) and X-ray diffraction measurements are reported elsewhere [12]. The typical number density of ZnO QDs as estimated from TEM micrograph was ~ 10^{13} /cm^2. A representative TEM image of ZnO QDs of mean size ~ 2 nm grown on Alumina buffer layer and corresponding selective area electron diffraction (SAED) pattern are shown in inset of Fig. T.2.5. The room temperature optical absorption spectra of ZnO QDs of mean sizes in the range of ~ 3 to 1.6 nm is shown in Fig. T.2.3, wherein a clear blue shift in ZnO absorption edge was observed with decreasing mean quantum dot size in line with putative quantum confinement effect [12].

The room temperature near band-edge PL spectra of ZnO QDs of different sizes in the range of ~3 to 1.6 nm are shown in Fig. T.2.4. For comparison, the PL spectrum of ~ 300 nm thick ZnO film grown under similar conditions is also shown in the same figure. It can be seen from Fig. T.2.4 that excitonic UV photoluminescence corresponding to bandgap was observed at room temperature in all the ZnO QD samples with PL peak position shifted towards higher energy with decreasing size of QDs [13]. The maximum blue shift up to 3.82 eV was observed for ZnO QDs of smallest mean size ~ 1.6 nm compared to bulk ZnO bandgap of ~3.3 eV. The UV PL is believed to originate from bound or localized excitons in ZnO QDs [13, 14]. It is well known that the exciton localization is strong enough in ZnO QDs that it can manifest itself even at room temperature [14]. It can also be seen that the UV PL peak broadened with decreasing size of the QDs which could be attributed to increase in size dispersion with decreasing mean size of QDs. Further it can be noticed that

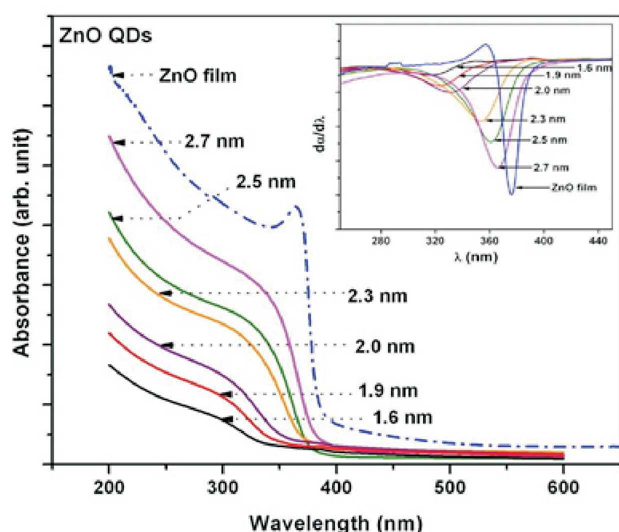

Fig. T.2.3:Room temperature optical absorption spectra of ZnO QDs of different sizes. Inset shows the first derivative of absorption spectra.

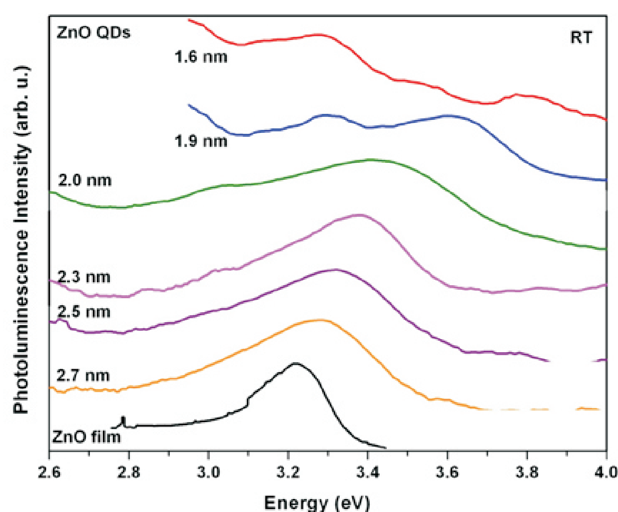

Fig. T.2.4: Room temperature near band-edge PL spectra of ZnO QDs of different sizes

below ~ 2 nm dot size (which is less than the reported exciton Bohr radius in ZnO ~ 2.1 nm), the variation in PL peak with size is strong compared to their larger counterparts along with emergence of an additional weak PL peak below the main peak. This relatively weak additional PL feature appearing below the main peak can be speculated to be due to the surface-bound impurity exciton complexes mainly due to the fact that its position is insensitive to size and below the confined exciton PL peak [14].

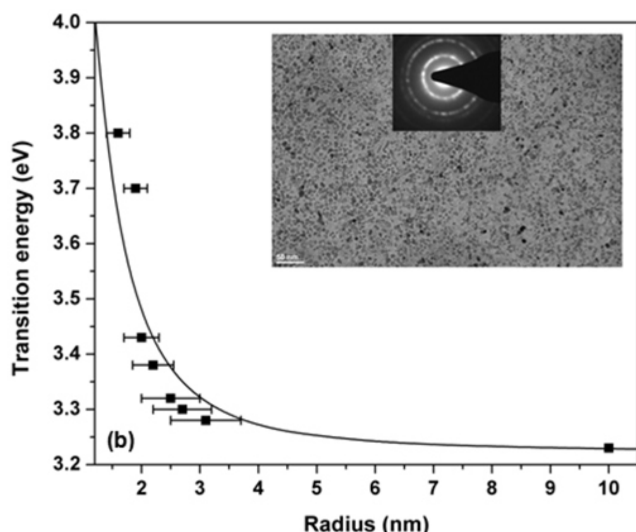

Fig. T.2.5: Variation of exciton transition energy as a function of radius of ZnO QDs. The continuous curve shows the results of variation calculation. Inset shows typical TEM micrograph and SAED pattern of ZnO QDs.

To confirm that the UV PL observed in ZnO QDs is due to quantum confinement of excitons, the ground state energy of excitons confined in ZnO quantum dots embedded in alumina matrix has been estimated using variational calculation [15]. The exciton-LO phonon interaction and finite depth of the potential well has been considered in the calculations. The ZnO QDs embedded in alumina matrix have been assumed as spherical quantum wells with the well depth obtained from the difference between the electron affinities of bulk Alumina and ZnO. The conduction band offset was 3.5 eV and valence band offset was 2.2 eV. Strong interaction between the excitons and optical phonons has taken into account using the Pollmann-Buttner effective potential between the electrons and holes. The asymmetry of the electron and hole masses has also been incorporated into the variational ansatz. The calculated value of ground state energy of excitons in ZnO QDs is shown in Fig. T.2.5 along with PL peak position observed experimentally. The calculated variation of ZnO bandgap with size matched quite well with those obtained experimentally from the PL data. Thus, it is concluded that the observed UV emission is intrinsically size dependent and arise due to quantum confinement of excitons. Armed with this growth methodology and size dependent root temperature PL data, one can deploy these ZnO QDs for UV light emitting applications.

3.2 $Mg_xZn_{1-x}O$/ZnO Heterostructures

Fabrication of device grade heterostructures of ZnO/MgZnO with physically and chemically sharp interfaces and good crystalline quality is essentials for development of quantum transport devices based on ZnO and its variants. Due to mismatch in macroscopic polarization between MgZnO and ZnO, when such heterostructures are grown along c-axis, a 2D electron gas results at the ZnO side of the interface [16, 17]. Recently there have been few reports on the realization of 2D electron gas at MgZnO/ZnO interface and associated quantum hall effect [18, 19], however studies on effect of defects and disorder on their transport properties are scanty.It is well expected that during deposition of MgZnO/ZnO heterostructures, Mg atoms from the MgZnO layer may diffuse to the ZnO side creating disorder. Furtherthe lattice mismatch between MgZnO and ZnO may introduce structural disorder at the interface. These defects and disorders act as scattering centers for 2D electrons and modify their transport characteristics. We found that when mean free path of 2D electrons reducesto values comparable to the Fermi wavelengthof the electron, interference effects become prominent and the conductivity gets modified due to quantum corrections [20]. The results of this study are briefly present below.

To study the effect of disorder on the transport characteristics of 2D electron gas in polar ZnO, the$Mg_xZn_{1-x}O$/ZnO heterostructures were grown by PLD using high temperature buffer assisted low temperature growth approach [21] in which first, about 80 nm thick film of ZnO was grown on sapphire at a growth temperature of ~ 750°C and subsequent MgZnO layer of ~ 50 nm thickness was grown at 400°C. Mg concentration (x) in $Mg_xZn_{1-x}O$ over layer was varied in the range of ~ 16 to 40% to optimize concentration of 2D electrons [20]. Resistivity and Hall measurements of these samples were carried out in the van der Pauw geometry. Isothermal magnetoresistance measurements were performed in the magnetic field range of 0 to 8 T.

The sheet resistance of the $Mg_xZn_{1-x}O$/ZnO heterostructures was found to decrease and sheet carrier density increase with increasing Mg concentration in the $Mg_xZn_{1-x}O$ layer as shown in Fig. T.2.6. Further the electron mobility was found to

increase initially with increasing Mg concentration. These are typical characteristics of 2D electron gas formed at the polar heterointerface [22, 23]. From Hall measurements it was also confirmed that the electron density was temperature independent signifying absence of carrier activation and formation of 2D electron gas. The mobility was found to be almost temperature independent at low temperatures in contrast to that of ZnO thin film, wherein the mobility decreased with decreasing temperature at low temperatures [20].

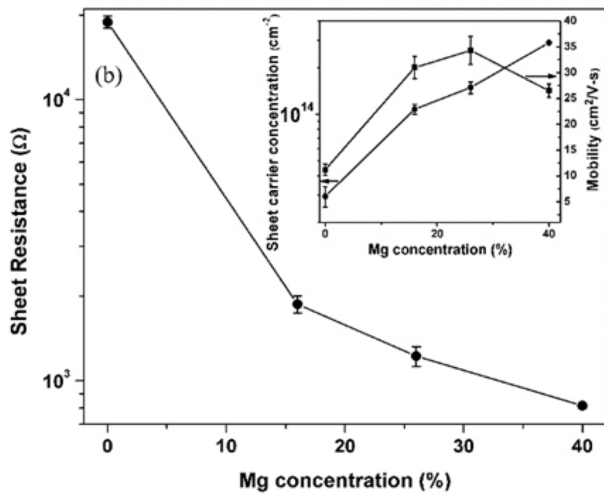

Fig. T.2.6: Variation of sheet resistance of $Mg_xZn_{1-x}O/ZnO$ heterostructures as a function of Mg concentration (x). The inset shows the variation of electron concentration and mobility as a function of Mg concentration (x).

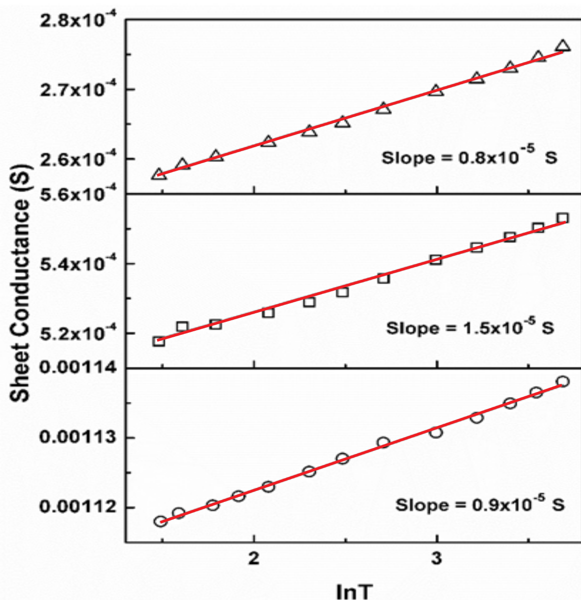

Fig. T.2.7: Sheet conductance as a function of ln (T) for $Mg_xZn_{1-x}O/ZnO$ heterostructures for x = 0.16 (triangles), x = 0.26 (squares), x = 0.4 (circles)

Temperature dependent resistivity measurements showed negative temperature coefficient of resistance of all the heterostructures at low temperatures. From isothermal magneto-resistance measurement it was found that all the films showed negative magneto-resistance, the magnitude of which decreased with increasing temperature. These observations of negative temperature coefficient of resistivity together with negative magnetoresistance are consistent with the phenomena of quantum corrections to conductivity which occurs because of electron interference effects [24]. In the heterostructures, indeed it was calculated that the electron mean free path was comparable to the Fermi wavelength [20]. In a 2D system, in presence of quantum corrections, the conductivity is expected to vary logarithmically with temperature which was observed in MgZnO/ZnO heterostructures as shown in Fig. T.2.7. The logarithmic variation of conductivity with temperature revealed that the quantum interference effects play a significant role in shaping up the low temperature transport properties of 2DEG formed at the MgZnO/ZnO interface. Further studies on the transport properties of 2DEG in ZnO are underway.

3.3 Ultra-thin films of high k gate oxide $LaGdO_3$:

In order to maintain the exponential growth of processing speed and component density, the feature sizes of metal-oxide-semiconductor (MOS) structures in logic devices and metal-insulator-metal (MIM) capacitors in memory devices are down scaled from one technology node to the other following Moore's Law [25]. According to the International Technology Roadmap for Semiconductors (ITRS) Process Integration, Devices, and Structures 2 (PIDS2) table for future high performance logic technology devices (based on extended planar bulk), an equivalent oxide thickness of 6.5 Å is required for 20 nm and below technology node [26]. Such a lower effective oxide thickness (EOT) may not be achieved by the presently used nitride hafnium silicate gate dielectrics due to their low permittivity ~ 12-15. The urgency and importance of this issue demands that new alternative materials with even higher dielectric constants (k>20), reduced loss tangent, and lower leakage currents should be developed to achieve long term goal. Recent studies by both academia and industry showed that rare-earth based multi-component oxides in the amorphous state are among the promising candidates for that purpose [27, 28]. We have used pulsed laser deposition to grow amorphous ultra-thin films of ternary interlanthenide oxides $LaGdO_3$, $SmGdO_3$ and $LaLuO_3$ with dielectric constant > 20 [29] and studied their electrical properties for advanced gate dielectric applications. A review of our studies on $LaGdO_3$ as gate dielectric is presented below :

Amorphous thin films of ($LaGdO_3$) LGO were fabricated on (100) p-Si substrates with~ 3-6 ohm-cm resistivity by using optimized PLD process [30]. The silicon substrates, before loading in to the PLD chamber were ultrasonicated in acetone and then in methanol and finally immersed in 2% $HF:H_2O$ solution for 30s to remove the native oxide. The LGO ceramic target was prepared in-house by pelletizing multiple calcined mixture of predetermined amount of high purity (~99.99%) La_2O_3 and Gd_2O_3 powders which was sintered at 1500 °C in air for 4 h. The target to substrate distance was kept at 5 cm. The substrates were heated up to the growth temperature of ~ 300 °C in vacuum, and high purity (99.99%) oxygen at a partial pressure of 1-2 mTorr was introduced in to the chamber just before deposition to minimize the duration of exposure of H-terminated Si wafer to oxygen ambient. The KrF excimer laser (248 nm, 1 Hz) with a fluence of ~3 J/cm^2 was used for ablation. LGO thin films of various thicknesses in the range of ~ 3-50 nm which was measured using glazing incidence X-ray reflectivity were grown on Si substrate. To grow Pt/LGO/Si n-MOS devices, about 50nm thin Pt gate metal electrodes of area ~ 2.5×10^5 cm^2 were deposited using dc sputtering at a power density of ~ 1W/cm^2 through square metal shadow. These devices were passivated using forming gas annealing treatment (90% N_2+ 10% H_2) at 400 °C for 20 min in rapid thermal annealing (RTA) chamber to reduce the interface trap density. The capacitance-voltage (C-V) sweep was carried out at 100 kHz (50mV AC drive signal) and C-V curves were modeled using Hauser CVC program [31]. Temperature-dependent gate oxide leakage measurements were carried out in the range of 300-450K to study current conduction mechanisms.

The C-V characteristics of Pt/LGO/p-Si MOS devices measured at a frequency of 100 kHz are depicted in Fig. T.2.8. As can be seen, the C-V curves show a counter-clockwise hysteresis during sweeping from inversion to accumulation (forward) and back to inversion (reverse). The observed hysteresis was larger for thicker gate oxide layers compared to the thinner ones and may be attributed to the presence of rechargeable oxide traps in the layer. The dielectric constant (k) value of the LGO layers was estimated to be 20.5 ± 2.4 from the accumulation capacitance density in terms of the EOT (without quantum mechanical correction) as a function of physical thickness as shown in inset (a) of Fig. T.2.8. It can also be concluded from the intercept on the EOT axis in the same inset that there exists an interfacial layer (perhaps of La-Gd silicate) having thickness 4.5 ± 1Å with moderate high-k value (~ 8-14) formed due to reaction between LGO and Si at the interface. It was observed that the thinner LGO films with EOT < 1.5 nm which were preserved in inert argon atmosphere, exhibited positive flat band voltage shift, indicating presence of negative charges in the form of interstitial oxygen (O_i^{2-}) in LGO while atmosphere exposed thicker films showed negative flat band voltage perhaps due to presence of positive oxide charges in the form of oxygen vacancies Vo^{2+}. The overall flat band voltage shift in both the cases was in the range of ± 0.5 V (roll-off and roll up). The EOT versus V_{fb} plot as shown in inset Fig. T.2.8(b) was found to fit to straight line indicating that dipoles at the high-k/Si interface are responsible for the V_{fb} shift and the fixed charge density Q_f estimated from slope of the linear fit was ~ 1.5×10^{12} / cm^2.

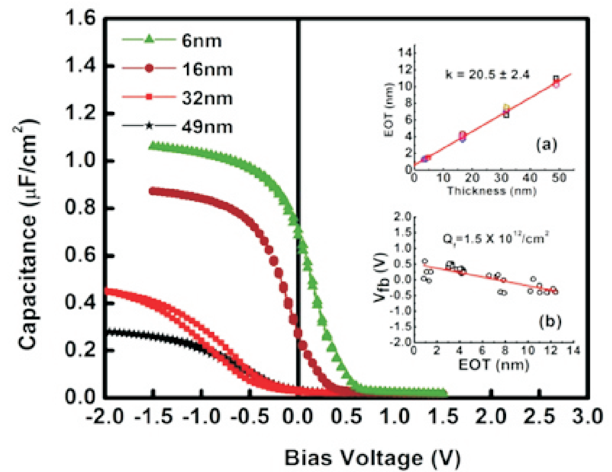

Fig. T.2.8: High-frequency C-V curves of Pt/LGO/Si gate stacks with LGO thicknesses from 6 to 49 nm. (a) The XRR thickness as a function of EOT (b) Flat band voltage versus EOT characteristics.

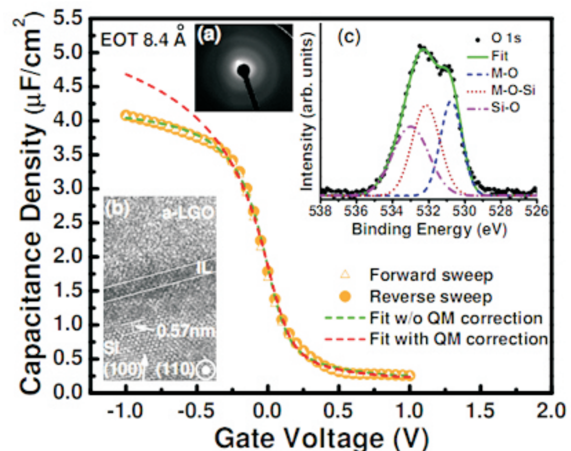

Fig. T.2.9: C-V characteristics of Pt/LGO/p-Si n-MOS deices measured at 100 kHz including its Hauser fit with and without quantum mechanical correction (a) SAED image of a-LGO. (b) Cross-sectional TEM images of LGO thin film. (c) O1s XPS peak from ~ 8 nm thick LGO layer on Si after Ar^+ sputtering etches.

Fig. T.2.9 shows the C-V curve of Pt/LGO/p-Si MOS device containing ultra-thin film of LGO having physical thickness ~ 3 nm. It can be seen that C-V characteristics of device is unsaturated (due to ultra-thinness) but close to ideal C-V curve with negligibly small hysteresis ~ 2 mV and interface trap density D_{it} 6 $\times 10^{12}$ cm^{-2} eV^{-1}. The EOT determined from the accumulation capacitance by fitting experimental C-V data to ideal simulation curve with and without quantum mechanical correction were ~ 5.4 Å and 8.4 Å respectively. Cross-sectional image of one of the heterostructures with ~8 nm thick LGO film studied using HRTEM (Fig. T.2.9(b)) revealed ~ 6 Å thin structure less interface layer IL between LGO layer and Si substrate. The SAED image (Fig. T.2.9 (a)) without any sharp rings or spots revealed amorphous nature of LGO layer. The XPS measurements (Fig. T.2.9(c)) confirmed formation of La-Gd silicates (dark layer) and silicon oxide (SiO_x) at interface. Analysis of temperature dependent leakage currents (please refer ref. 29 for details) revealed that gate injection current was dominated by Schottky emission below 1.2 MV/cm and quantum mechanical tunneling above this field. Our studies clearly revealed that LGO could be a promising candidate for the future sub-nanometer logic technology nodes, especially with gate last sequence, by incorporating high-aspect ratio geometries.

3.4 Resistive memory switching materials

Resistive memory switching in thin films of metal oxides have recently shown tremendous potential to overcome the physical and technological limitations of existing CMOS based memory technology discussed above [32- 34]. The resistive switching (RS) memory devices store information through transition between two states of resistances (low and high) on application of bias voltage in contrast to CMOS based nonvolatile memory which is based on charge-storage. Among other materials being explored for RS application, oxides which are compatible with existing CMOS technology such as TiO_2, Ta_2O_5, HfO_2, NiO etc., and rare earth ternary oxides are preferred. The unipolar resistive switching in these metal oxide films has been attributed to the formation and dissolution of nano sized conductive filaments (CF) across the oxide layer which mainly comprises of oxygen vacancies and metallic ions [32-34]. However, some of the prevailing issues in resistive switching memories are lack of information on RS time, i.e. how fast is switching process from one state to other state, and capability of multiple bit storage in same memory element. We have addressed these issues in our Lab. and observed that multiple nonvolatile resistance states with reasonably good resistance contrast can be obtained in thin films of amorphous ternary inter-lanthanides $LaGdO_3$ and $SmGdO_3$ by precisely controlling the compliance current during switching event. Details of these studies can be found in our publications (29, 35).

As discussed above, one of the important concerns in unipolar resistive memory switching in NiO thin film is lack of information on RS time and its dependence on other switching parameters. We have investigated the dynamic processes during RS of NiO thin film to evaluate RS time and its dependence on compliance current [36]. For these studies ~ 20 nm thick polycrystalline NiO films were grown on commercial $Pt/TiO_2/SiO_2/Si$ substrates using optimized PLD. Top electrodes of ~ 50 nm thick Au film with a typical diameter of ~ 200 μm were used to construct Au/NiO/Pt metal-insulator-metal structures. Nonvolatile unipolar RS was repeatedly observed in these devices through current-voltage measurements in top-bottom configuration on application of suitable electrical bias as shown in Fig. T.2.10.

To measure the switching time of RS events namely set (switching from high to low resistance state) and reset (switching from low to high resistance state) processes, the required voltage pulse with predetermined pulse width was applied using Keithley source meter and a digital storage oscilloscope (400 MHz, LeCroy make) was used to record both the voltage pulse applied across the device and current flowing through device simultaneously. The dynamic evolution of set and reset events have been clearly seen in Fig. T.2.11 from which the set and reset times have been evaluated to be ~ 10ns and ~ 150μs for compliance current of ~ 5mA. Repeatedly the set process was found to be much faster (~ 10^4 times) than reset process. However, as the compliance current was increased from ~ 5 to 75 mA, the reset time increased monotonically from ~ 150μs to ~ 3ms while set time remained nearly unaffected and varied randomly in the range of ~ 10-20 ns without any specific dependence on compliance current.

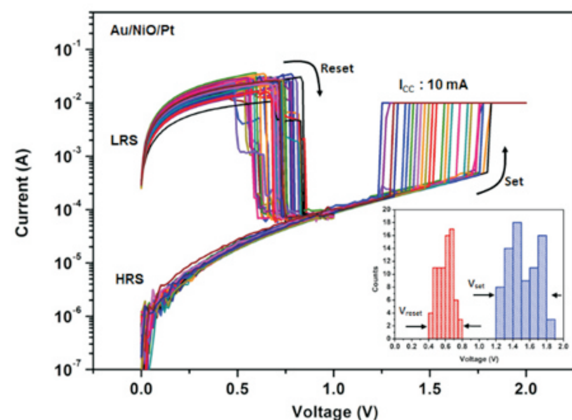

Fig. T.2.10: I-V plot of Au/NiO/Pt device showing repetitive nonvolatile resistance switching. Inset shows set and reset voltage dispersion.

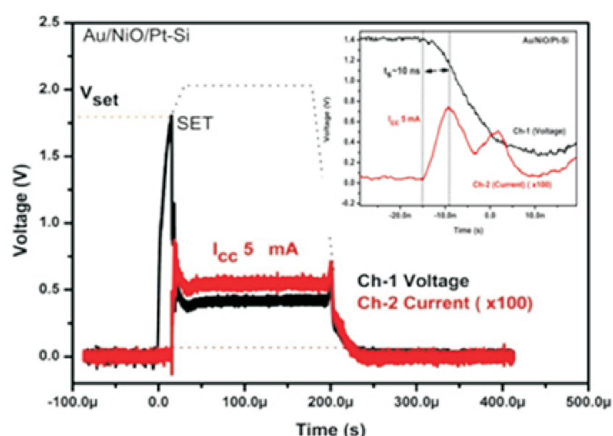

Fig. T.2.11: Voltage vs time plot of (upper) set and (lower) reset switching processes. Ch-1 shows the applied voltage pulse across the Au/NiO/Pt device and Ch-2 shows the measured current pulse. Inset in upper figure shows zoomed current and voltage for the set switching.

The observed variation in reset time and insensitivity of set time on varying compliance current could be understood in light of conductive filamentary model where size i.e., diameter of CFs increases with increasing compliance current [29, 37]. This in-turn may lead to relatively larger time required for rupture of thicker CFs through Joule heating. The increase in size of CFs with increasing compliance current was supported by decrease in resistance of device and temperature coefficient of resistance (α) with increasing compliance current. Our studies on dynamical processes of resistive switching in NiO films clearly show that resistive switching memories are potential candidate for fast nonvolatile data storage applications.

4. Conclusions

In conclusion, we have used KrF excimer laser based PLD process to deposit technologically advanced materials including multilayered stacks of ZnO quantum dots separated by Alumina matrix which showed size dependent blue shift in bandgap due to putative quantum confinement effect and efficient excitonic photoluminescence in UV spectral range at room temperature. We have also deposited high quality MgZnO/ZnO heterostructures with different Mg concentrations and observed quantum corrections to conductivity of 2D electon gas due to weak localization and electron electron interference effects which are important for development of transparent electronic devices based on 2D electron gas. Further, we have deposited ultrathin films of rare earth high k dielectric oxide $LaGdO_3$ and observed EOT ~ 0.65 with low leakage current which has direct implication in scaling of MOS based logic and memory devices below 22 nm technology nodes. In addition, amorphous metal oxides have been grown by optimized PLD where in multilevel nonvolatile resistance switching and switching time of the order of ~ 10 ns have been observed which are important observations towards realization of fast nonvolatile memory based on resistance change. Our recent studies clearly show that PLD is a versatile tool to grow device grade nanostructures of technologically important oxide materials with high throughput.

Acknowledgements

Authors would like to acknowledge Dr. A. K. Das, Dr. R. S. Ajimsha and Shri V. K. Sahu of LMPD for their contribution towards this work. Authors are grateful to Prof. L. M. Kukreja for his keen interest and deep association with pulsed laser deposition activity at RRCAT. Authors are also thankful to colleagues at LMPD and other divisions of RRCAT who have been associated at various stages of this work. One of the authors (PM) is particularly thankful to Prof. R. S. Katiyar, University of Puerto Rico, San Juan, USA for his association and many fruitful discussions on RHEED monitored PLD process and high k-dielectric related work.

References

[1] Thin Film Growth Techniques for Low-Dimensional Structures, R. F. C. Farrow, S. S. P. Parkin, P. J. Dobson, J. H. Neave, A. S. Arrott;,Springer US (1987)

[2] Pulsed Laser Deposition of nanostructured semiconductors, L. M. Kukreja, B. N. Singh and P. Misra, BOTTOM-UP NANOFABRICATION, K. Ariga and H. S. Nalwa (Eds.), American Scientific, California, Chapter 9, pp. 235 – 274 (2009)

[3] Pulsed Laser Deposition of thin films, Douglas B Chrisey and Graham K. Hubler (Eds.), John Wiley & Sons, Inc., New York, p 23 (1994)

[4] Pulsed Laser Deposition of Thin Films: Applications-Led Growth of Functional Materials, Robert Eason, Wiley-Interscience (2006)

[5] Excimer Lasers, P. W. Hoff, C. K. Rhodes, Springer Berlin Heidelberg (1979)

[6] H. H. Kim, S. Park, Y.Yi, D. I. Son, C. Park, D. K. Hwang, and W. K. Choi, Scientific Reports 5, 1-5 (2015)

[7] J. Chen, J. Pan, D. Qingguo, G. Alagappan, Q. W. Lei, X. L. Jun, Appl. Phys. A 117: 589 (2014)

[8] M. H. Crawford, IEEE J. Select. Top. Quant. Electron. 15, 1028 (2009)

[9] P. Misra, T. K. Sharma, S. Porwal and L. M. Kukreja, Appl. Phys. Lett. 89, 161912 (2006)

[10] C.F. Klingshirn, A. Waag, A. Hoffmann, J. Geurts, Zinc Oxide: From Fundamental Properties Towards Novel Applications, Springer Series in Materials Science, Springer (2010)

[11] A. F. Vladimir and A. A. Balandina, Appl. Phys. Lett. 85, 5971(2004)

[12] L. M. Kukreja, P. Misra, A. K. Das, J. Sartor, H. Kalt, J. Vac. Sci. Technol. A 29, 03A120 (2011)

[13] P. Misra, A. K. Das, M. P. Joshi, B. Singh and L. M. Kukreja, 24Th DAE-BRNS National Laser Symposium (NLS-24), Raja Ramanna Centre for Advanced Technology, Indore, December 2-5, 2015

[14] V. A. Fonoberov and A. A. Balandin, Appl. Phys. Lett. **85**, 5971 (2004)

[15] R. T. Senger and K. K. Bajaj, Phys. Rev. B 68, 045313 (2003)

[16] J. Falson, Y. Kozuka, M. Uchida, J. H. Smet, T. Arima, A. Tsukazaki and M. Kawasaki, Scientific Reports 6, 26598 (2016)

[17] O. Ambacher, J. Smart, J. R. Shealy, N. G. Weimann, K. Chum, M. Murphy, W. J. Schaff, L. F. Eastman, R. Dimitrov, L. Wittmer, M. Stutzmann, W. Rieger, and J. Hilsenbeck: J. Appl. Phys. **85**, 3222 (1999).

[18] A. Tsukazaki, S. Akasaka, K. Nakahara, Y. Ohno, H. Ohno, D. Maryenko, A. Ohtomo, M. Kawasaki, Nature Materials 9, 889–893 (2010)

[19] W. Luo and T. Chakraborty, Phys. Rev. B **93**, 161103 (2016)

[20] A. K. Das, P. Misra, R. S. Ajimsha, M. P. Joshi, L. M. Kukreja, Appl. Phys. Lett. 107 (10), 102104 (2015)

[21] P. Misra and L.M. Kukreja, Thin Solid Films, 485, 42 (2005)

[22] F. Bernardini, V. Fiorentini, and D. Vanderbilt: Phys. Rev. B **56**, R10024 (1997)

[23] H.-A. Chin, I-C. Cheng, C.-I Huang, Y.-R. Wu, W.-S. Lu, W.-L. Lee, J. Z. Chen, K.-C. Chiu, and T.-S. Lin, J. Appl. Phys **108**, 054503 (2010)

[24] V. F. Gantmakher, Electrons and Disorder in Solids, Oxford Science Publications, Oxford (2005).

[25] G. E. Moore G. E., Cramming more components onto integrated circuits, Electronics, Magazine **38**, No. 8, April 19, (1965).

[26] International Technology Roadmap for Semiconductors (Semiconductor IndustryAssociation 2013); see http:/www.itrs.net for updates.

[27] Lanthanide-Based High-k Gate Dielectric Materials, D. J. Lichtenwalner, Springer Series in Advanced Microelectronics 43, pp 343-369, Springer (2013)

[28] Yi Zhao, Materials 5, 1413-1438 (2012)

[29] P. Misra, Y. Sharma, G. Khurana, R.S. Katiyar, Emerging Materials Research 4 (1), 18-31(2015)

[30] S.P. Pavunny, P. Misra, R. Thomas, A. Kumar, J. Schubert, J.F. Scott, and R.S. Katiyar, Appl. Phys. Lett. 102 (19), 192904-192904-5 (2013)

[31] J. R. Hauser, IEEE Trans. Electron Devices 43, 1981 (1996)

[32] R. Waser and M. Aono, Nat. Mater., **6**, 833 (2007) .

[33] G. I. Meijer, Science **319**, 1625 (2008) .

[34] K. M. Kim, G. H. Kim, S. J. Song, J. Y. Seok, M. H. Lee, J. H. Yoon, and C. S. Hwang, Nanotechnology **21**, 305203 (2010) .

[35] Y. Sharma, P. Misra, S. P. Pavunny, R. S Katiyar, Appl. Phys. Lett. 104 (7), 73501 (2014)

[36] P. Misra, V. K. Sahu, R S Ajimsha, A. K. Das, B. Singh, *Proceed.* IUMRS-International Conference of Young Researchers on Advanced Materials (IUMRS-ICYRAM 2016), IISc Bangalore, Dec. 10-15, (2016).

[37] A. Bid, A. Bora, and A. K. Raychaudhuri, Phys. Rev. B 74, 035426 (2006)